Low-Complexity FNN-Based Transmit Antenna Selection for Enhanced Performance in VASM Systems over Rician Fading Channels

Tran Viet Vinh, Pham Thanh Hiep, Nguyen Thu Phuong
Advanced Wireless Communications Group, Le Quy Don Technical University, Ha Noi, Viet Nam.

Correspondence: Nguyen Thu Phuong: E-mail: phuong.nt@lqdtu.edu.vn
Communication: received xxx, revised xxx, accepted xxx
DOI: 10.32913/mic-ict-research.v2025.n1.1346

***Abstract*: Variable Active Antenna Spatial Modulation (VASM) is a spatial modulation variant designed to improve spectral efficiency and offer greater flexibility in system configuration. In this paper, we propose a feedforward neural network (FNN) framework to address the transmit antenna selection (TAS) problem, aiming to enhance performance in VASM systems operating over Rician fading channels. Computational results demonstrate that our novel FNN-TAS algorithm provides a significant reduction in computational costs compared to the standard Euclidean distance-based method. Additionally, simulation results indicate that the bit error rate (BER) of the VASM system increases with the Rician factor. However, the proposed FNN-TAS method effectively improves BER performance for VASM systems, particularly at high Rician factors, and outperforms conventional TAS methods based on channel gain.**

Index Terms: *Variable active antenna spatial modulation (VASM), antenna selection (TAS), feedforward neural network (FNN), Euclidean distance-based TAS (ED-TAS), Rician fading channel.*

I. Introduction

Driven by the rapid advancement of sixth-generation (6G) wireless technology [1], future communication systems must meet unprecedented requirements, including ultra-high data rates, ultra-low latency, and seamless connectivity. Achieving these goals while ensuring spectral and energy efficiency is crucial for the sustainable and scalable deployment of next-generation networks.

Among the key technologies shaping 6G, Multiple-Input Multiple-Output (MIMO) has been widely recognized for its ability to enhance spectral efficiency, improve signal reliability, and support massive connectivity [2]. Within the broader family of multi-antenna transmission techniques, Spatial Modulation (SM) [3] has gained increasing attention due to its ability to reduce hardware complexity while maintaining high spectral efficiency, making it a promising candidate for energy-efficient next-generation systems [4].

In SM systems, the bitstream is divided into equally sized groups, with each group further split into two parts. The first part selects an Amplitude and Phase Modulation (APM) symbol, while the second part activates an antenna index to transmit the selected APM symbol. Due to this straightforward operational principle, SM systems enhance spectral efficiency, reduce inter-antenna interference, and minimize radio frequency chain requirements.

Unlike conventional spatial modulation systems, such as SM, Generalized SM (GSM) [5], and Quadrature SM (QSM) [6], which activate a fixed number of transmit antennas (TAs) in a time slot, Variable Active Antenna Spatial Modulation (VASM) [7] is an SM variant that offers the flexibility to vary the quantity of active TAs. This approach further enhances spectral efficiency while reducing the number of required TAs. Additionally, VASM enables more straightforward TA configuration selection, as the TA count is not restricted to powers of two. VASM thus presents itself as a promising candidate for high-speed wireless systems with flexible antenna usage [8–11].

In MIMO systems applying spatial modulation principles, a portion of the information is conveyed through the indices of the active TAs. Studies have shown that increasing the number of TAs can enhance spectral efficiency, but it may come at the cost of increased BER [4]. In MIMO systems with a large number of TAs, potentially reaching hundreds (massive MIMO [12]), using all TA indices to transmit additional information through SM principles is impractical, as this would result in an excessively high BER, compromising system quality. Moreover, each TA corresponds to a unique transmission channel, potentially offering varying transmission effectiveness. Therefore, selecting the appropriate TAs for modulation and signal transmission is crucial in systems operating on SM principles like VASM.

Various antenna selection techniques have been proposed to address this critical aspect in family SM systems [13–16]. Channel-Gain-based TAS (CG-TAS) as well as Euclidean distance-based TAS (ED-TAS) [13] are two fundamental techniques underpinning most TAS schemes for SM and its variants. CG-TAS selects TAs based on their channel gains, while ED-TAS uses an exhaustive search to optimize the Euclidean distance between transmit signals, resulting in the best BER performance.

To reduce the computational complexity of ED-TAS while maintaining near-optimal BER performance, various antenna selection strategies have been proposed for VASM systems. One such strategy, the hierarchical approach combining CG-TAS together with ED-TAS, termed HC-TAS, is presented in [17–19]. This algorithm offers a flexible trade-off between computational complexity and BER performance, adapting to diverse system requirements.

The Rician fading channel is a widely observed propagation model in wireless communications, characterized by the presence of a dominant line-of-sight (LoS) component alongside multiple weaker multipath components [20]. This channel model is particularly relevant in scenarios where a strong direct transmission path coexists with scattered reflections, such as in satellite communications, urban mobile networks, and millimeter-wave systems.

However, previous studies [21–23] have demonstrated that the BER performance of spatial modulation-based systems significantly degrades in Rician fading channels as the Rician factor increases. This degradation occurs because, in scenarios where the LoS component is dominant, the receiver faces increased difficulty in distinguishing which antenna transmitted the signal, leading to a higher probability of antenna index detection errors. In such conditions, conventional TAS schemes that rely on channel gain metrics, such as CG-TAS and HC-TAS, may become ineffective in Rician fading environments. This challenge underscores the necessity of developing advanced TAS techniques tailored to the unique characteristics of Rician channels to maintain robust system performance.

Recently, several studies have explored the use of neural networks to replace traditional TAS methods for SM family systems [24–28]. These approaches have shown promising improvements in performance metrics. For example, studies such as [24, 25] proposed using deep neural networks (DNNs) for TAS and signal detection in SM-MIMO systems, achieving near-optimal BER performance with low computational complexity. Three typical DNNs—feedforward neural networks (FNN), convolutional neural networks (CNN), and recurrent neural networks (RNN)—have been employed for TAS in SM-MIMO systems [26] and for fully generalized spatial modulation (FGSM) systems in [27]. These studies demonstrated that leveraging DNNs for TAS can significantly reduce computational burden while improving BER performance.

However, these prior works have primarily focused on minimizing computational complexity and achieving near-optimal BER performance under Rayleigh fading channel conditions. As far as we are aware, no existing study has explored TAS under Rician fading conditions, which are commonly encountered in practical scenarios, or within VASM systems.

Additionally, CNNs are particularly effective for spatially correlated data due to their ability to extract local features, while RNNs excel at modeling sequential data owing to their capacity to retain temporal dependencies. For data such as random wireless channels, where spatial and temporal correlations are minimal or nonexistent, FNNs are a practical and efficient choice [29].

For these reasons, in this paper, we propose employing an FNN-based TAS approach for VASM systems operating over Rician fading channels.

The main contributions of this paper can be summarized as follows:

- This paper develops an FNN structure for efficient antenna selection in VASM systems, achieving notable computational complexity reductions over the optimal ED-TAS method and delivering improved BER performance relative to CG-TAS and HC-TAS under high Rician factor conditions.
- We propose five distinct techniques for constructing datasets to train neural networks for antenna selection and compare the effectiveness between them.
- We calculate and compare computational complexity to demonstrate the superiority of FNN-based TAS (FNN-TAS) over ED-TAS.
- Reliable simulation results are presented to evaluate the influence of the Rician factor and the efficacy of various TAS techniques on the BER performance of VASM systems employing the proposed methods.

The remainder of the paper is organized as follows: Section II presents the VASM system model with TAS and the Rician channel model. Section III details the antenna selection method using FNN. Simulation results are provided in Section IV. Section V concludes the paper and suggests future research directions.

Notations: The notations used throughout this paper are defined as follows. Italic lowercase letters represent variables, while bold uppercase letters denote matrices, and bold lowercase letters signify vectors. The notation $(\bullet)^T$

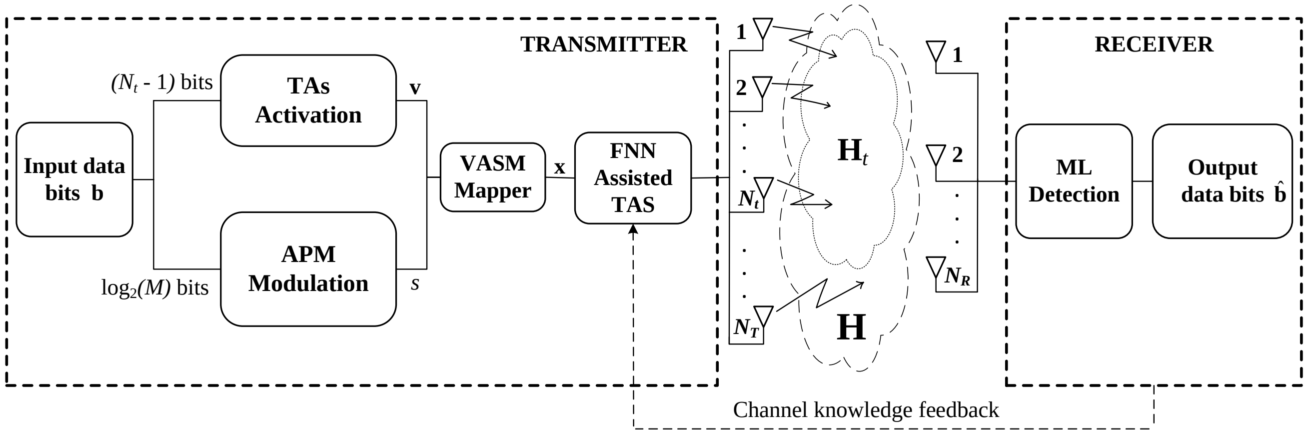

Figure 1. VASM system architecture incorporating TAS.

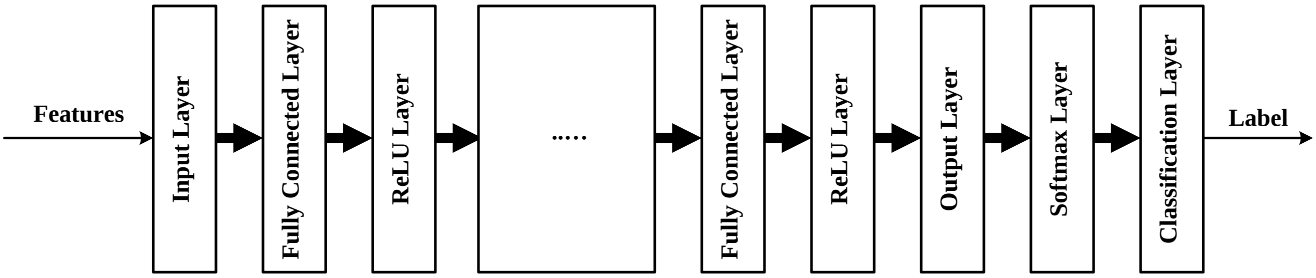

Figure 2. Proposed FNN architecture.

is used for the transpose operation, and $(\bullet)^H$ indicates the Hermitian transpose operation. The symbol $\|\bullet\|$ denotes the calculation of a norm. A matrix of size $A \times B$ is represented by $\mathbb{C}^{A\times B}$, and C_b^a signifies the combination of a elements chosen from b elements. Finally, the expectation operator is denoted by $\mathbb{E}[\bullet]$.

II. System Model

The VASM transceiver model [11] incorporating FNN-TAS is illustrated in Fig. 1. This model differs from previous VASM models by employing FNN-TAS for transmit antenna selection instead of traditional methods [17].

In this setup, the transmitter is equipped with N_T TAs, but only N_t of these TAs are actively used for data transmission, where $N_t < N_T$. On the receiver side, there are N_R receive antennas (RAs). The channel between the transmitter and receiver is represented by the channel matrix $\mathbf{H} \in \mathbb{C}^{N_R\times N_T}$. When N_t TAs are selected, the channel matrix is reduced to an effective channel matrix $\mathbf{H}_t \in \mathbb{C}^{N_R\times N_t}$, obtained by selecting the corresponding columns of $\mathbf{H}$.

This study considers the Rician fading channel model, which is widely used to describe environments where a strong LoS component is present alongside several scattered non-LoS (NLoS) paths. This channel can be mathematically expressed as the sum of a deterministic LoS component $\mathbf{H}_{\text{LoS}} \in \mathbb{C}^{N_R\times N_T}$ and a stochastic NLoS component $\mathbf{H}_{\text{NLoS}} \in \mathbb{C}^{N_R\times N_T}$ with $\mathcal{CN}(0,1)$. The channel model is given by [20]:

$$\mathbf{H} = \sqrt{\frac{K}{K+1}}\mathbf{H}_{\text{LoS}} + \sqrt{\frac{1}{K+1}}\mathbf{H}_{\text{NLoS}}, \tag{1}$$

here K is Rician factor that represents the power ratio of the LoS to NLoS components.

In the system, the receiver first estimates the channel state information (CSI) and feeds this information return to the transmitter. Utilizing the received channel knowledge, the transmitter selects N_t TAs out of the total available N_T TAs to transmit the data, aiming to maximize the quality of the signal and thus improve the overall system performance.

The input data bit sequence b is segmented into groups of fixed length $(N_t-1)+\log_2(M)$ bits, where M denotes the modulation order of the APM scheme. Each group is then divided into two parts: the first part, comprising N_t-1 bits, represents the spatial bits, while the second part, containing $\log_2(M)$ bits, represents the symbol bits.

The spatial bits specify the activation states of the TAs, with a bit value of 1 indicating an active TA and a bit value of 0 indicating an inactive one. In cases where all spatial bits are 0, the last TA within the chosen set of N_t TAs is activated. The remaining $\log_2(M)$ bits are modulated into an APM symbol, $s_m \in \mathbb{S}$, $m \in [1; M]$, which is then mapped to the positions of the active TAs, forming the transmitted VASM signal vector $\mathbf{x} \in \mathbb{X}$.

Using the above simple mapping principle, VASM activates between 1 and $N_t - 1$ TAs to emit signals within a single time slot, achieving a spectral efficiency of $\log_2(M)+ (N_t - 1)$ bits per channel use. Consequently, it can operate with an unrestricted number of TAs, achieving considerably greater spectral efficiency in comparison to other SM family variants [18].

The received signal vector $\mathbf{y} \in \mathbb{C}^{N_R \times 1}$ is represented as follows:

$$\mathbf{y} = \sqrt{\gamma}\mathbf{H}_t\mathbf{x} + \mathbf{n}, \tag{2}$$

here $\mathbf{n} \in \mathbb{C}^{N_R \times 1}$, $\mathcal{CN}(0, 1)$, represents the additive white Gaussian noise (AWGN) vector. γ represents the average signal-to-noise ratio (SNR) at the receiver.

With the assumption of perfect CSI knowledge at the receiver, the received signal is detected using optimal maximum likelihood detection [30], leading to the following expression:

$$\widehat{\mathbf{x}} = \underset{\mathbf{x} \in \mathbb{X}}{\operatorname{argmin}} \left\| \mathbf{y} - \sqrt{\gamma}\mathbf{H}_t\mathbf{x} \right\|^2, \tag{3}$$

here $\hat{\mathbf{x}}$ denotes the estimated transmitted signal. $\hat{\mathbf{x}}$ is, finally, mapped back to the original data bits.

III. Transmit Antenna Selection

In a VASM-MIMO system, there are a total of N_T TAs at the transmitter, but the number of available radio frequency chains is $N_f < N_T$. The required number of TAs to be selected for transmission is $N_t = N_f$. The TAS problem can thus be defined as the task of selecting N_t columns out of the N_T columns of the channel matrix $\mathbf{H}$ with the best quality for signal transmission.

1. Conventional transmit antenna selection methods

a) Transmit antenna selection based on channel gain

The CG-TAS method is a selection algorithm that chooses the best N_t TAs out of N_T TAs based on the criterion of maximizing individual channel gains. In particular, the usage channel matrix $\mathbf{H}_t^{\mathrm{CG}}$ is constructed by choosing N_t columns from the channel matrix $\mathbf{H}$, as follows:

$$\mathbf{H}_t^{\mathrm{CG}} = \begin{bmatrix} \mathbf{h}_1 & \mathbf{h}_2 & \cdots & \mathbf{h}_{N_t} \end{bmatrix}. \tag{4}$$

These columns are selected by sorting the column norms in descending order:

$$||\mathbf{h}_1|| > ||\mathbf{h}_2|| > \cdots > ||\mathbf{h}_{N_t}|| > \cdots > ||\mathbf{h}_{N_T}||. \tag{5}$$

b) Transmit antenna selection using Euclidean distance

The ED-TAS approach is an optimization algorithm designed to identify the optimal subset of TAs that maximizes the minimum Euclidean separation between transmitted signal vectors, thereby enhancing system performance.

$$\mathbf{H}_t^{\mathrm{ED}} = \arg \max_{c \in [1; C_{N_T}^{N_t}]} \{ \min_{\mathbf{x}_i \neq \mathbf{x}_j \in \mathbb{X}} ||\mathbf{H}_t^c(\mathbf{x}_i - \mathbf{x}_j)||^2 \}. \tag{6}$$

c) Combination of CG-TAS and ED-TAS in a hierarchical structure

The HC-TAS approach employs a sequential two-stage process to select the optimal subset of TAs. In the initial stage, a subset of N_s TAs with the highest channel gains is chosen from the total N_T TAs, forming a reduced channel matrix $\mathbf{H}_{N_s}^{\mathrm{CG}}$:

$$\mathbf{H}_{N_s}^{\mathrm{CG}} = \begin{bmatrix} \mathbf{h}_1 & \mathbf{h}_2 & \cdots & \mathbf{h}_{N_s} \end{bmatrix}, \tag{7}$$

where the columns are sorted in descending order of their norm. Subsequently, the ED-TAS algorithm is applied to the reduced set of N_s TAs to select the final N_t TAs, as expressed by the following optimization problem:

$$\mathbf{H}_t^{\mathrm{HC}} = \arg\max_{d \in [1; C_{N_s}^{N_t}]} \min_{\mathbf{x}_i \neq \mathbf{x}_j \in \mathbb{X}} ||\mathbf{H}_t^d(\mathbf{x}_i - \mathbf{x}_j)||^2. \tag{8}$$

Thus, the HC-TAS method effectively leverages CG-TAS for coarse-grained selection and ED-TAS for fine-grained optimization.

2. Feedforward neural network-based transmit antenna selection

a) FNN architecture design

The proposed FNN architecture is illustrated in Fig. 2. It consists of several sequential layers, including an input layer, an output layer, and fully connected hidden layers. The network begins with an input layer that receives the feature vector, followed by some fully connected (dense) layers, each activated by a rectified linear unit (ReLU) layer to introduce non-linearity. The output from the final dense layer is passed to an output layer with a Softmax function to compute a probability distribution across classes, assigning the class with the highest probability as the final prediction. This architecture enables the FNN to learn complex patterns within the input data, facilitating accurate classification.

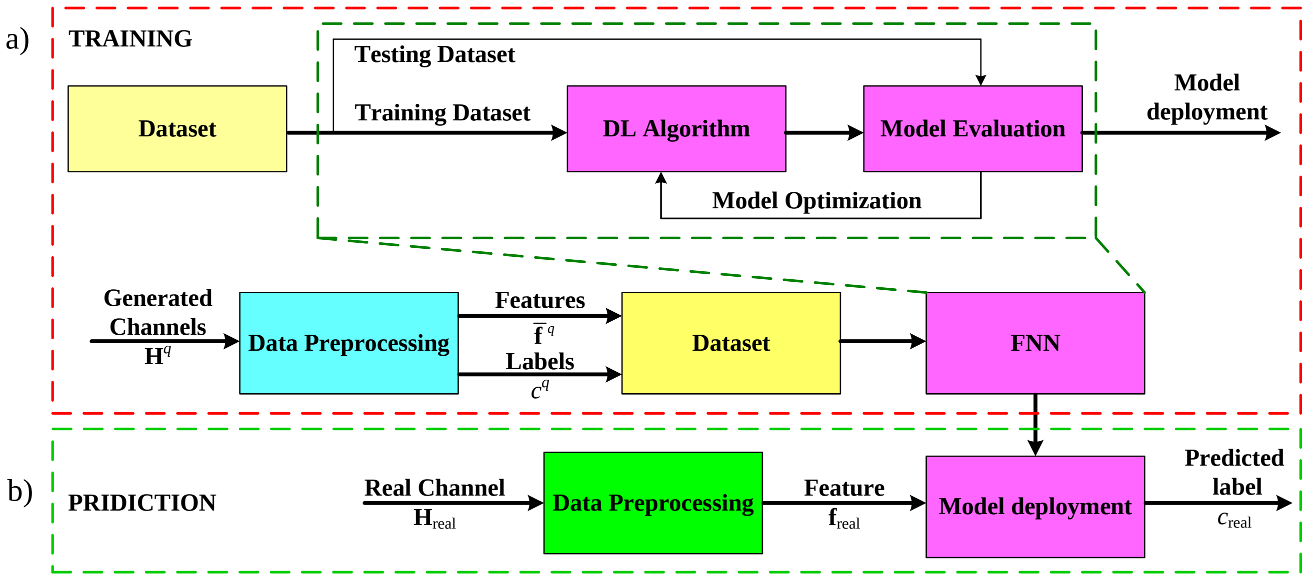

Figure 3. Training and prediction procedure of proposed FNN.

b) Preparation of training data

To create the training dataset, the channel matrices with complex values must be transformed into real-valued feature vectors compatible with FNN input requirements. The steps for preparing the training data are as follows:

- ***Step 1***: Generate a total of Q random channel matrices $\mathbf{H}^q$, where $1 \leq q \leq Q$, as given in (1).
- ***Step 2***: Feature extraction from each channel matrix $\mathbf{H}^q$. In this study, we derive five distinct feature types from $\mathbf{H}^q$, each representing different channel attributes. The extraction process for these features is outlined below:

  - Real and imaginary components (R&I):

$$\mathbf{f}^q_{\text{R\&I}} = \left[\Re(h^q_{1,1}), \Im(h^q_{1,1}), \ldots, \Re(h^q_{N_R,N_T}), \Im(h^q_{N_R,N_T})\right], \tag{9}$$

  where $h^q_{a,b}$, with $1 \leq a, b \leq N_T$, is the (a,b)-th entry of $\mathbf{H}^q$.

  - Magnitude (Mag):

$$\mathbf{f}^q_{\text{Mag}} = [|h^q_{1,1}|, |h^q_{1,2}|, \ldots, |h^q_{N_R,N_T}|], \tag{10}$$

  with $|h^q_{a,b}| = \sqrt{\Re(h^q_{a,b})^2 + \Im(h^q_{a,b})^2}$.

  - Norm (Norm):

$$\mathbf{f}^q_{\text{Norm}} = \left[||\mathbf{h}^q_1||, ||\mathbf{h}^q_2||, \ldots, ||\mathbf{h}^q_{N_T}||\right]. \tag{11}$$

  - Phase (Phase):

$$\mathbf{f}^q_{\text{Phase}} = \left[\angle(h^q_{1,1}), \angle(h^q_{1,2}), \ldots, \angle(h^q_{N_R,N_T})\right], \tag{12}$$

  where $\angle(h^q_{a,b}) = \tan^{-1}\left(\frac{\Im(h^q_{a,b})}{\Re(h^q_{a,b})}\right)$.

  - Correlation (Corr):

$$\mathbf{f}^q_{\text{Corr}} = \left[|\mathbf{h}^q_1{}^H \mathbf{h}^q_1|, |\mathbf{h}^q_1{}^H \mathbf{h}^q_2|, \ldots, |\mathbf{h}^q_{N_T}{}^H \mathbf{h}^q_{N_T}|\right]. \tag{13}$$

  After obtaining the features, normalization is performed to prevent bias effects. Max-min normalization is applied as follows:

$$\bar{\mathbf{f}}^q = \frac{\mathbf{f}^q - \mathbb{E}[\mathbf{f}^q]}{\mathbf{f}_{\max} - \mathbf{f}_{\min}}, \tag{14}$$

  where $\mathbf{f}_{\min} = \min(\mathbf{f}^1, \mathbf{f}^2, \ldots, \mathbf{f}^Q)$ and $\mathbf{f}_{\max} = \max(\mathbf{f}^1, \mathbf{f}^2, \ldots, \mathbf{f}^Q)$ are the minimum and maximum values of the features, respectively.
- ***Step 3***: Labeling. Each label c^q corresponds to the index of the optimal TA combination, derived based on the following criterion:

$$c^q = \underset{c \in [1; C^{N_t}_{N_T}]}{\arg\max} \left\{ \min_{\mathbf{x}_i \neq \mathbf{x}_j \in \mathbb{X}} ||\mathbf{H}^q_{t,c}(\mathbf{x}_i - \mathbf{x}_j)||^2 \right\}, \tag{15}$$

  where $\mathbf{H}^q_{t,c} \in \mathbb{C}^{N_R \times N_t}$ are the sub-channel matrices generated by selecting N_t columns from the N_T columns in $\mathbf{H}^q \in \mathbb{C}^{N_R \times N_T}$.

As a result, the training dataset is composed of two parts: the feature vector set $\mathbb{F} = \{\bar{\mathbf{f}}^1, \bar{\mathbf{f}}^2, \ldots, \bar{\mathbf{f}}^Q\}$ and the associated label vector $\mathbf{c} = \{c^1, c^2, \ldots, c^Q\}$. The neural network is trained to map these features to labels by minimizing a loss function, allowing it to predict optimal antenna configurations in real-world channel scenarios.

c) Training and testing

Figure 3a provides a detailed illustration of the training process of the proposed FNN. Initially, a dataset comprising generated channel realizations $\mathbf{H}^q$ undergoes preprocessing to extract relevant feature vectors and their corresponding labels. For each channel matrix $\mathbf{H}^q$, a feature vector $\mathbf{f}^q$ is extracted based on one of the expressions from (9) to (13), depending on the selected feature extraction technique, and is subsequently normalized according to (14) to obtain $\overline{\mathbf{f}}^q$. The corresponding label c^q is determined using (15). During training, the neural network learns the mapping relationship between the feature vector $\overline{\mathbf{f}}^q$ and the label c^q. The dataset is then divided into a training set and a testing set, where the former is used for parameter optimization, while the latter is employed to assess model generalization. The training dataset is fed into a deep learning algorithm, which iteratively updates the network parameters through an optimization process. The trained model is subsequently validated using the testing dataset, and performance evaluation is conducted to ensure satisfactory accuracy. Once optimal performance is achieved, the trained model is deployed for real-time inference.

d) Prediction

Figure 3b demonstrates the prediction (inference) phase of the deployed FNN. In this phase, the real channel matrix $\mathbf{H}_{\text{real}}$, representing the actual communication environment, undergoes the same preprocessing steps as in the training phase to extract the feature vector $\mathbf{f}_{\text{real}}$. This feature vector is then fed into the trained FNN model, which predicts the label c_{real}. This label corresponds to the optimal set of transmitting antennas for the current channel conditions, thereby facilitating enhanced transmission performance in practical scenarios.

3. Computational complexity

In this study, we define the computational complexity of TAS methods as the number of floating-point operations (flops) required to determine the TA combination for the VASM system.

According to the analysis results in [17, 18], the computational complexity of conventional TAS methods can be expressed as:

$$\Omega_{\text{CG-TAS}} = N_T(4N_R - 1) + N_T N_t - \frac{N_t(N_t+1)}{2} \tag{16}$$

$$\Omega_{\text{ED-TAS}} = C_{N_T}^{N_t} \times \left(\frac{2^{2\varepsilon} - 2^{\varepsilon}}{2} \times (8N_R N_t + 2N_R - 1) + 1\right) - 1, \tag{17}$$

$$\Omega_{\text{HC-TAS}} = N_T(4N_R - 1) + N_T N_s - \frac{N_s(N_s+1)}{2} + C_{N_s}^{N_t} \times \left(\frac{2^{2\varepsilon} - 2^{\varepsilon}}{2} \times (8N_R N_t + 2N_R - 1) + 1\right) - 1. \tag{18}$$

Here, $\varepsilon = (N_t - 1) + log_2(M)$ is the spectral efficiency of VASM.

For FNN-TAS, since the training process is conducted offline, the computational complexity of FNN-TAS is the sum of the flops from the data preprocessing step on real channel and the flops from the FNN prediction phase. However, the feature extraction process requires a relatively small number of flops compared to the prediction phase, and thus its computational cost can be neglected. Assuming the FNN has L hidden layers, with the number of neurons in each layer denoted as $[n_1, n_2, ..., N_L]$ the computational complexity of the prediction phase in the FNN is the total number of dot-product operations and activations across each layer. The total number of flops for the entire FNN is given by [25]:

$$\text{flop}_{\text{FNN}} = n_{\text{in}} n_1 + n_1 + \sum_{l=1}^{L-1} (n_l \; n_{l+1} + n_{l+1}) + n_L n_{\text{out}} + n_{\text{out}}, \tag{19}$$

where n_{in} and n_{out} are the number of neurons in the input and output layers of the FNN, respectively.

Since different feature extraction techniques lead to varying computational complexities for the data preprocessing step and input size (n_{in}), we calculate the computational complexity of FNN-TAS for the five proposed feature extraction methods as follows:

$$\Omega_{\text{FNN-TAS (R \& I)}} = 2N_R N_T n_1 + n_1 + \sum\nolimits_{l=1}^{L-1} (n_l n_{l+1} + n_{l+1}) + n_L n_{\text{out}} + n_{\text{out}}, \tag{20}$$

$$\Omega_{\text{FNN-TAS (Mag)}} = N_R N_T n_1 + n_1 + \sum\nolimits_{l=1}^{L-1} (n_l n_{l+1} + n_{l+1}) + n_L n_{\text{out}} + n_{\text{out}}, \tag{21}$$

$$\Omega_{\text{FNN-TAS (Phase)}} = N_R N_T n_1 + n_1 + \sum\nolimits_{l=1}^{L-1} (n_l n_{l+1} + n_{l+1}) + n_L n_{\text{out}} + n_{\text{out}}, \tag{22}$$

$$\Omega_{\text{FNN-TAS (Norm)}} = N_T n_1 + n_1 + \sum\nolimits_{l=1}^{L-1} (n_l n_{l+1} + n_{l+1}) + n_L n_{\text{out}} + n_{\text{out}}, \tag{23}$$

$$\Omega_{\text{FNN-TAS (Corr)}} = {N_T}^2 n_1 + n_1 + \sum\nolimits_{l=1}^{L-1} (n_l n_{l+1} + n_{l+1}) + n_L n_{\text{out}} + n_{\text{out}}, \tag{24}$$

Table I
SIMULATION PARAMETERS FOR THE SYSTEM.

Parameter	Value
Total number of TAs	$N_T = 10$
Number of TAs selected	$N_t = 3$
Number of temporary TAs in HC-TAS	$N_s = 4, 5, 6$
Number of RAs	$N_R = 4$
APM modulation level	$M = 4$ (QPSK)

Table II
TRAINING HYPERPARAMETERS OF THE FNN

Hyperparameter	Value
Sample size (Q)	10^5
Holdout ratio	80-20%
Optimizer	Adam
Activation function	ReLU
Max epochs	500
Mini batch size	64
Initial learn rate	0.00015

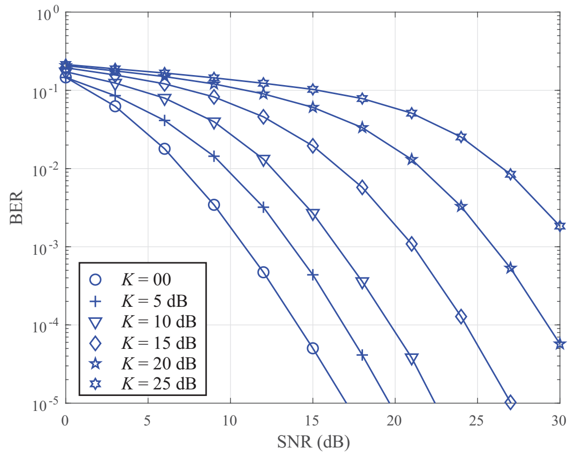

Figure 4. BER performance of the VASM system with Ran-TAS versus SNR for $K = 0 : 25$ dB.

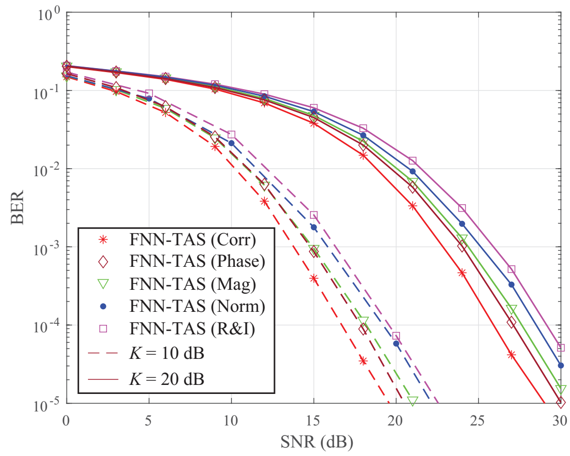

Figure 5. Comparison of the efficiency of feature extraction techniques through the BER performance of the VASM system employing FNN-TAS.

Equations (20) through (24) clearly show that the computational complexity of the proposed FNN-TAS scheme depends only on the total number of TAs, the number of RAs, and the architecture of the neural network. Importantly, it is unaffected by both the count of selected TAs and the modulation order of APM.

IV. SIMULATION RESULTS AND DISCUSSIONS

This section presents simulations of the VASM system, employing the previously discussed TAS techniques under various Rician channel coefficients, to assess the effectiveness of the proposed FNN-TAS approach. For clarity, the simulation parameters used are listed in Table I and II. Ran-TAS refers to the method of randomly selecting N_t TAs from a total of N_T TAs.

1. Investigation of the impact of Rician factor on BER performance of VASM systems

It can be observed from Fig.4 that the system's BER performance declines with increasing K-factor. The reason is that, with a higher K-factor, the LoS component becomes dominant, causing the differences between the channel paths to become smaller. As a result, the receiver has more difficulty distinguishing which TAs transmitted the signal. This reduces the accuracy of TAs index detection, which, in turn, leads to an increased BER. These results are fully consistent with those reported in [21–23].

2. Assessment of the effectiveness of feature extraction techniques

The paper extracted five important channel features to create the training dataset. However, it is unclear which feature will yield the best performance. Therefore, in this subsection, we evaluate the BER performance achieved by FNN-TAS using five datasets generated by extracting these five channel features. For this analysis, we employ an FNN (64/32/16) with $K = 10$ dB and $K = 20$ dB. The results in Fig. 5 indicate that FNN-TAS (Corr) achieves the best BER performance, followed by FNN-TAS (Phase), FNN-TAS (Mag), FNN-TAS (Norm), and finally, FNN-TAS (R&I). This demonstrates that the correlation feature among the columns of the channel matrix contains valuable information that enhances the learning capability of the FNN more effectively than the other features. Based on these results, we will focus on using dataset extracted by this feature in subsequent simulations.

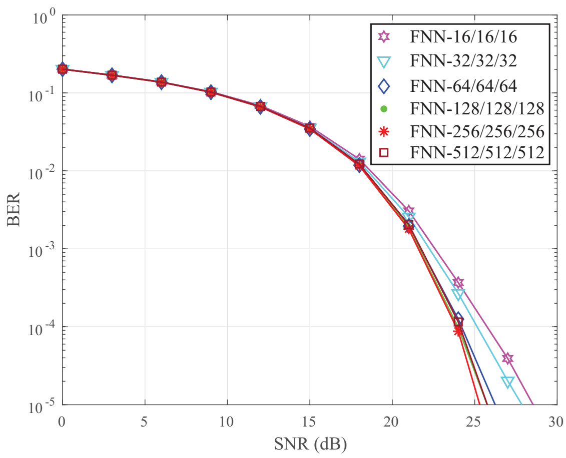

Figure 6. FNN-TAS BER performance in VASM system for different hidden layer setups at K = 20 dB.

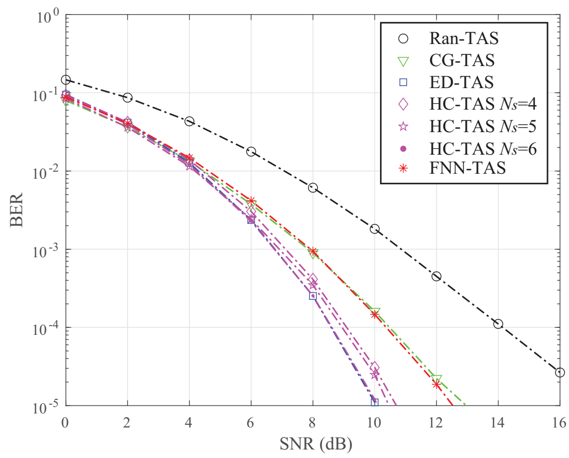

Figure 7. Comparison of BER performance enhancement achieved by TAS methods in VASM system at K = 0.

3. Evaluation of BER performance of FNN-TAS with different network configurations

Figure 6 illustrates the BER performance results of the FNN-TAS-VASM system, where neural networks with different numbers of hidden neurons share a common dataset extracted from correlation features between the columns of the channel matrix, with K = 20 dB. It is evident that as the number of hidden neurons increases, the BER performance improves significantly. However, when the network configuration changes from 256/256/256 to 512/512/512, the BER performance not only fails to improve but even degrades, whereas the computational complexity increases significantly. Therefore, the FNN (256/256/256) configuration can be considered an optimal choice for subsequent simulations.

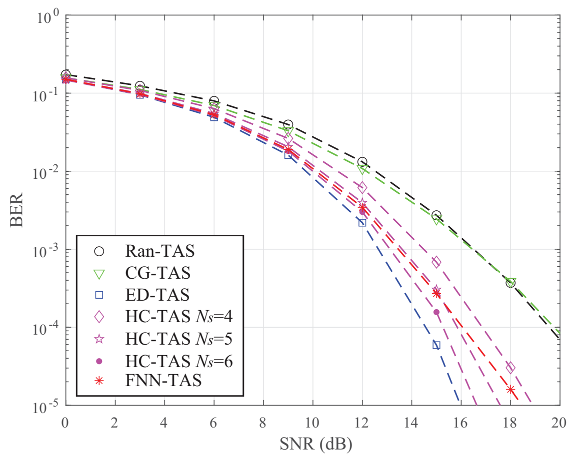

Figure 8. Comparison of BER performance for VASM systems employing various TAS techniques at K=10 dB.

4. BER performance evaluation of TAS-VASM systems under varying Rician factors

In Figs. 7, 8, and 9, we compare the BER performance of the VASM system achieved by the proposed FNN-TAS (256/256/256) and traditional TAS selection methods at K-factors of 0 (Rayleigh channel), 10 dB, and 20 dB. The results show that as the K-factor increases, the system's BER performance deteriorates for all TAS methods. However, the introduced FNN-TAS consistently surpasses CG-TAS, Ran-TAS, and even HC-TAS (N_s = 4 and K = 10 dB), with a lower rate of degradation. Notably, in Fig. 9, at the higher K-factor of 20 dB, the BER performance of FNN-TAS surpasses HC-TAS ($N_s = 4, 5, 6$) and nearly matches the optimal performance of ED-TAS.

This result clearly demonstrates that FNN-TAS performs effectively in Rician channel conditions with high Rician factors. The reason is that under high Rician factor conditions, the transmission channel is relatively stable, facilitating feature extraction and learning from the characteristics by the FNN. Consequently, higher performance is achieved.

5. Computational complexity comparison

Based on expressions from (16) to (24), along with the system parameters outlined above and the FNN (256/256/256), we have determined the computational complexity of the TAS algorithms, as illustrated in Fig. 10. The various feature extraction techniques result in disparate levels of computational complexity, albeit the differences are not significant. Notably, the FNN-TAS approach requires substantially less computational burden in comparison with ED-TAS and is comparable to HC-TAS.

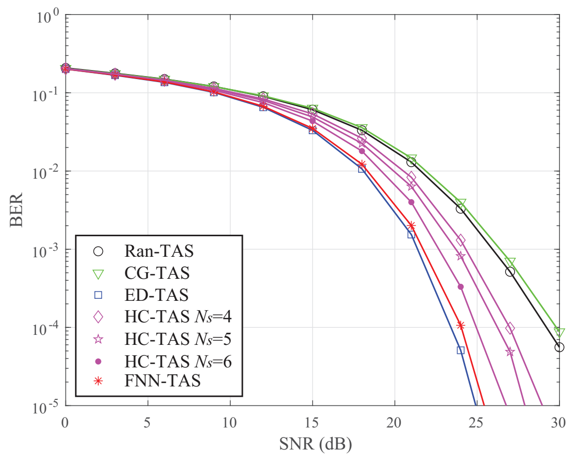

Figure 9. BER performance comparison of VASM systems using different TAS approaches at K=20 dB.

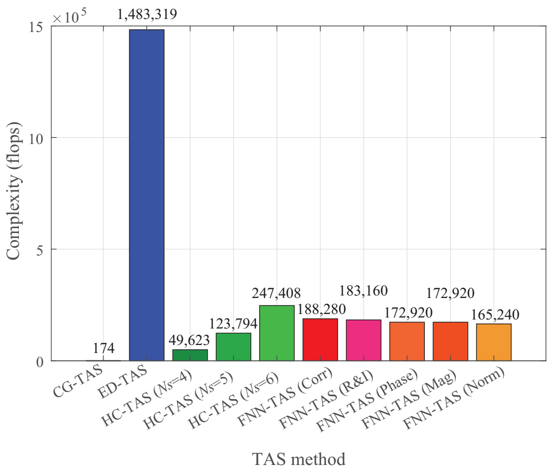

Figure 10. Computational complexity of TAS methods.

These results suggest that FNN-TAS is a favorable option for TAS in VASM systems under Rician fading channels, as it balances computational complexity with significant improvements in BER performance.

V. Conclusion and Future Works

This paper proposed the FNN-TAS scheme for VASM systems under Rician fading channels, achieving low complexity while maintaining superior BER performance. The proposed scheme demonstrates notable advantages in Rician channels with a dominant LoS component, providing valuable insights into TAS design tailored to channel conditions. Performance evaluations indicate that correlation-based features between channel matrix columns are the most informative for FNN training. Additionally, an optimal configuration with 256 neurons per hidden layer achieves a favorable trade-off between computational complexity and classification accuracy. The proposed FNN-TAS outperforms conventional HC-TAS and CG-TAS while closely approximating ED-TAS performance at a significantly reduced computational cost.

In future research, we will focus on extending FNN-TAS to low-latency applications, such as intelligent transportation and UAV communications. Furthermore, the potential of advanced neural network architectures for TAS in multi-antenna systems will be explored to enhance both efficiency and adaptability.

References

[1] M. N. A. Siddiky, M. E. Rahman, M. S. Uzzal, and H. M. D. Kabir, "A comprehensive exploration of 6G wireless communication technologies," *Computers*, vol. 14, no. 1, Jan. 2025.

[2] Z. Wang, J. Zhang, H. Du, D. Niyato, S. Cui, B. Ai, M. Debbah, K. B. Letaief, and H. V. Poor, "A tutorial on extremely large-scale MIMO for 6G: Fundamentals, signal processing, and applications," *IEEE Communications Surveys and Tutorials*, vol. 26, no. 3, pp. 1560–1605, Jan. 2024.

[3] R. Y. Mesleh, H. Haas, S. Sinanovic, C. W. Ahn, and S. Yun, "Spatial modulation," *IEEE Transactions on Vehicular Technology*, vol. 57, no. 4, pp. 2228–2241, Jul. 2008.

[4] M. Wen, B. Zheng, K. J. Kim, M. Di Renzo, T. A. Tsiftsis, K.-C. Chen, and N. Al-Dhahir, "A survey on spatial modulation in emerging wireless systems: Research progresses and applications," *IEEE Journal on Selected Areas in Communications*, vol. 37, no. 9, pp. 1949–1972, Sep. 2019.

[5] A. Younis, N. Serafimovski, R. Mesleh, and H. Haas, "Generalised spatial modulation," in *2010 Conference Record of the Forty Fourth Asilomar Conference on Signals, Systems and Computers*, Apr. 2010, pp. 1498–1502.

[6] R. Mesleh, S. S. Ikki, and H. M. Aggoune, "Quadrature spatial modulation," *IEEE Transactions on Vehicular Technology*, vol. 64, no. 6, pp. 2738–2742, Jun. 2015.

[7] O. Osman, "Variable active antenna spatial modulation," *IET Microwaves, Antennas and Propagation*, vol. 9, Oct. 2015.

[8] Y. Li, X. Lei, Y. Xiao, X. Zhou, and H. Niu, "Variable active pre-coding aided spatial modulation," in *2019 IEEE 19th International Conference on Communication Technology (ICCT)*. IEEE, Otc. 2019, pp. 670–673.

[9] S. Gadhai and R. Budhiraja, "Joint-mapping-based variable active antenna spatial modulation," *IEEE Wireless Communications Letters*, vol. 9, no. 10, pp. 1668–1672, Oct. 2020.

[10] T. V. Vinh, P. T. Hiep, and N. T. Phuong, "Combined variable active antenna spatial modulation and NOMA to enhance spectral efficiency for multiple users MIMO systems," in *2022 International Conference on Advanced Technologies for Communications (ATC)*, Nov. 2022, pp. 29–34.

[11] F. Zhu, H. Hai, Y. Peng, J. Hou, and X.-Q. Jiang, "Extended variable active antenna generalized spatial modulation," *IEEE Wireless Communications Letters*, vol. 13, no. 2, pp. 265–269, Feb. 2024.

[12] J. Zheng, J. Zhang, H. Du, D. Niyato, B. Ai, M. Debbah, and K. B. Letaief, "Mobile cell-free massive MIMO: Challenges, solutions, and future directions," *IEEE Wireless Communications*, Feb. 2024.

[13] R. Rajashekar, K. Hari, and L. Hanzo, "Antenna selection in spatial modulation systems," *IEEE Communications Letters*, vol. 17, no. 3, pp. 521–524, Jan. 2013.

[14] P. Yang, Y. Xiao, Y. L. Guan, S. Li, and L. Hanzo, "Transmit antenna selection for multiple-input multiple-output spatial modulation systems," *IEEE Transactions on Communications*, vol. 64, no. 5, pp. 2035–2048, Mar. 2016.

[15] R. Zhu, H. Chen, Y. Xiao, X. Ji, W. Tang, and Y. Zhao, "Reduced-complexity transmit antenna selection for spatial modulation," in *2020 IEEE 20th International Conference on Communication Technology (ICCT)*, Oct. 2020, pp. 888–892.

[16] G. Altın, "A novel and low-complexity algorithm of EDAS for spatial modulation systems," *IEEE Communications Letters*, vol. 24, no. 12, pp. 2922–2925, Aug. 2020.

[17] T. V. Vinh, A. H. Phan, N. T. Thanh, and N. T. Phuong, "Proposal of a hierarchical combination of CG-TAS and ED-TAS to improve BER performance at low complexity for VASM systems," in *2023 12th International Conference on Control, Automation and Information Sciences (ICCAIS)*. IEEE, Jan. 2024, pp. 448–453.

[18] T. V. Vinh, N. H. Minh, P. T. Hiep, and N. T. Phuong, "Transmit antenna selection for multi-user VASM systems: Simplicity and fairness," *AEU-International Journal of Electronics and Communications*, vol. 170, p. 154842, Oct. 2023.

[19] K. X. Thuc, T. V. Vinh, P. L. Nguyen, T. Van Luyen, H. M. Kha, and N. T. Phuong, "Investigation of transmit antenna selection for MU-VASM systems over correlated channels," in *International Conference on Ad Hoc Networks*. Springer, Mar. 2024, pp. 112–124.

[20] W. C. Jakes and D. C. Cox, *Microwave mobile communications*. Wiley-IEEE press, 1994.

[21] M. Xie, X. Yu, J. Chen, and T. Teng, "BER performance of unmanned aerial vehicle assisted spatial modulation system in Rician channels," *Physical Communication*, vol. 49, p. 101471, Dec. 2021.

[22] A. Kabil, A. Bendary, A. F. Darwesh, and H. Dahshan, "Spatial index modulation in fading channels: A fair comparison approach," in *2024 14th International Conference on Electrical Engineering (ICEENG)*, Jun. 2024, pp. 300–304.

[23] S. Shrestha, S. Naser, L. Bariah, S. Muhaidat, P. C. Sofotasios, H. Elgala, and E. Damiani, "Autoencoder-based spatial modulation for the next generation of wireless networks," *IEEE Internet of Things Journal*, vol. 11, no. 22, pp. 36 322–36 334, Nov. 2024.

[24] Y. Zhang, J. Wang, X. Wang, Y. Xue, and J. Song, "Efficient selection on spatial modulation antennas: Learning or boosting," *IEEE Wireless Communications Letters*, vol. 9, no. 8, pp. 1249–1252, Apr. 2020.

[25] A. Mohamed, Z. Bai, F.-P. Oloruntomilayo, K. Pang, Y. Yang, D. Zhou, and K. S. Kwak, "Low complexity deep neural network based transmit antenna selection and signal detection in SM-MIMO system," *Digital Signal Processing*, vol. 130, p. 103708, Sep. 2022.

[26] G. Altın and İ. A. Arslan, "Joint transmit and receive antenna selection for spatial modulation systems using deep learning," *IEEE Communications Letters*, vol. 26, no. 9, pp. 2077–2080, Jun. 2022.

[27] H. K. Jadhav and V. B. Kumaravelu, "Deep learning-assisted transmit antenna classifiers for fully generalized spatial modulation: Online efficiency replaces offline complexity," *Applied Sciences*, vol. 13, no. 8, p. 5134, Apr. 2023.

[28] F. Zhu, H. Hai, and X.-Q. Jiang, "Efficient antenna selection for adaptive enhanced spatial modulation: A deep neural network approach," *IEEE Communications Letters*, vol. 27, no. 5, pp. 1352–1356, May. 2023.

[29] H. Zhang and N. Yang, *Deep Learning in Wireless Communications*. Springer, 2025.

[30] A. Bhowal and R. S. Kshetrimayum, *Advanced spatial modulation systems*. Springer, 2021.

Tran Viet Vinh received a B.S. degree in Telecommunication Technological Command at Telecomunications University, Vietnam, in 2011, and an MS degree in Electronics Engineering from Le Quy Don Technical University, Vietnam, in 2017. He is currently studying for a Ph.D degree at Le Quy Don Technical University, Vietnam. His research interests include MIMO systems, spatial modulation, and antenna selection, deep learning for wireless communications.
E-mail: tranvietvinhsqtt@lqdtu.edu.vn

Pham Thanh Hiep received a B.E. degree in Communications Engineering from the National Defense Academy, Japan, in 2005; and received the M.E. and Ph.D. degrees in Physics, Electrical and Computer Engineering from Yokohama National University, Japan, in 2009 and 2012, respectively. He worked as an associate researcher at Yokohama National University, Yokohama, Japan, from 2012 to 2015. Now, he is a lecturer at Le Quy Don Technical University, Ha Noi, Vietnam. His research interests lie in the area of wireless communication technologies and signal processing.
E-mail: thanhhiep@lqdtu.edu.vn

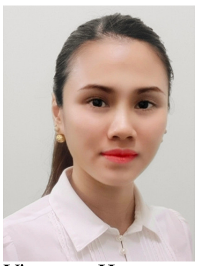

Nguyen Thu Phuong received the B.S, M.S and PhD degrees from Le Quy Don Technical University, Vietnam in 2008, 2012 and 2016, respectively. She is now a lecturer at Faculty of Radio-Electronics Engineering, and a significant member of the Advanced Wireless Communication Group, Le Quy Don Technical University, Hanoi, Vietnam. Her research interests are in the area of emerging technologies for future wireless communications: Energy harvesting, Non-orthogonal multiple access (NOMA), space-time processing, space-time coding, spatial modulation and index modulation, and massive MIMO systems.
E-mail: phuong.nt@lqdtu.edu.vn